

Diversity can be Transferred: Output Diversification for White- and Black-box Attacks

Yusuke Tashiro^{123*}, Yang Song¹, Stefano Ermon¹

¹Department of Computer Science, Stanford University, Stanford, CA, USA

²Mitsubishi UFJ Trust Investment Technology Institute, Tokyo, Japan

³Japan Digital Design, Tokyo, Japan

{ytashiro,yangsong,ermon}@cs.stanford.edu

Abstract

Adversarial attacks often involve random perturbations of the inputs drawn from uniform or Gaussian distributions, e.g. to initialize optimization-based white-box attacks or generate update directions in black-box attacks. These simple perturbations, however, could be suboptimal as they are agnostic to the model being attacked. To improve the efficiency of these attacks, we propose Output Diversified Sampling (ODS), a novel sampling strategy that attempts to maximize diversity in the target model’s outputs among the generated samples. While ODS is a gradient-based strategy, the diversity offered by ODS is transferable and can be helpful for both white-box and black-box attacks via surrogate models. Empirically, we demonstrate that ODS significantly improves the performance of existing white-box and black-box attacks. In particular, ODS reduces the number of queries needed for state-of-the-art black-box attacks on ImageNet by a factor of two.

1 Introduction

Deep neural networks have achieved great success in image classification. However, it is known that they are vulnerable to adversarial examples [1] — small perturbations imperceptible to humans that cause classifiers to output wrong predictions. Several studies have focused on improving model robustness against these malicious perturbations. Examples include adversarial training [2, 3], input purification using generative models [4, 5], regularization of the training loss [6–9], and certified defenses [10–12].

Strong attacking methods are crucial for evaluating the robustness of classifiers and defense mechanisms. Many existing adversarial attacks rely on random sampling, i.e., adding small random noise to the input. In white-box settings, random sampling is widely used for random restarts [13–16] to find a diverse set of starting points for the attacks. Some black-box attack methods [17, 18] also use random sampling to explore update directions for finding or improving adversarial examples. In these attacks, random perturbations are typically sampled from a naïve uniform or Gaussian distribution in the input pixel space.

Random sampling in the input space, however, may not sufficiently explore the output (logits) space of a neural network — diversity in the input space does not directly translate to diversity in the output space of a deep nonlinear model. We illustrate this phenomenon in the left panel of Figure 1. When we add random perturbations to an image in the input space (see dashed blue arrows in the first plot of Figure 1), the corresponding output logits could be very similar to the output for the original image (as illustrated by the second plot of Figure 1). Empirically, we observe that this phenomenon can negatively impact the performance of attack methods.

To overcome this issue, we propose a sampling strategy designed to obtain samples that are diverse in the output space. Our idea is to perturb an input away from the original one as measured directly by

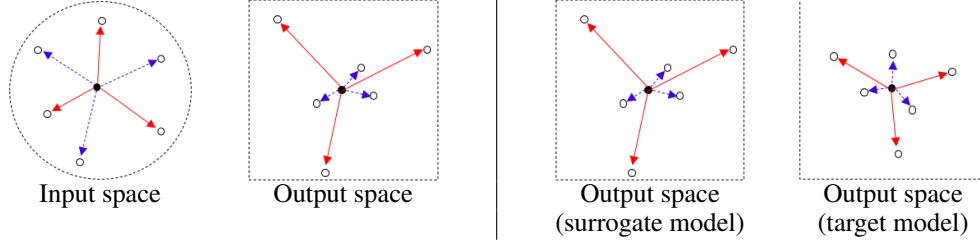


Figure 1: Illustration of the differences between random sampling (blue dashed arrows) and ODS (red solid arrows). In each figure, the black ‘o’ corresponds to an original image, and white ‘o’s represent sampled perturbations. (Left): white-box setting. Perturbations by ODS in the input space are crafted by maximizing the distance in the output space. (Right): black-box setting. Outputs on a target model correspond to perturbations crafted on a surrogate model.

distances in the output space (see solid red arrows in the second plot in Figure 1). First, we randomly specify a direction in the output space. Next, we perform gradient-based optimization to generate a perturbation in the input space that yields a large change in the specified direction. We call this new sampling technique Output Diversified Sampling (ODS).

ODS can improve adversarial attacks under both white-box and black-box settings. For white-box attacks, we exploit ODS to initialize the optimization procedure of finding adversarial examples (called ODI). ODI typically provides much more diverse (and effective) starting points for adversarial attacks. Moreover, this initialization strategy is agnostic to the underlying attack method, and can be incorporated into most optimization-based white-box attack methods. Empirically, we demonstrate that ODI improves the performance of ℓ_∞ and ℓ_2 attacks compared to naïve initialization methods. In particular, the PGD attack with ODI outperforms the state-of-the-art MultiTargeted attack [16] against pre-trained defense models, while its computational complexity is 50 times smaller on CIFAR-10.

In black-box settings, we cannot directly apply ODS because we cannot access gradients of the target model. As an alternative, we apply ODS to surrogate models and observe that the resulting samples are diverse with respect to the target model: diversity in the output space transfers (see the rightmost plot in Figure 1). Empirically, we demonstrate that ODS can reduce the number of queries needed for a score-based attack (SimBA [18]) by a factor of two on ImageNet, and also achieve better query-efficiency than the state-of-the-art Square Attack [19]. In addition, ODS with a decision-based attack (Boundary Attack [17]) reduces the median perturbation distances of adversarial examples by a factor of three compared to the state-of-the-art HopSkipJump [20] and Sign-OPT [21] attacks.

2 Preliminaries

We denote an image classifier as $f : x \in [0, 1]^D \mapsto z \in \mathbb{R}^C$, where x is an input image, z represents the logits, and C is the number of classes. We use $h(x) = \arg \max_{c=1, \dots, C} f_c(x)$ to denote the model prediction, where $f_c(x)$ is the c -th element of $f(x)$.

Adversarial attacks can be classified into targeted and untargeted attacks. Given an image x , a label y and a classifier f , the purpose of untargeted attacks is to find an adversarial example x^{adv} that is similar to x but causes misclassification $h(x^{adv}) \neq y$. In targeted settings, attackers aim to change the model prediction $h(x^{adv})$ to a particular target label $t \neq y$. The typical goal of adversarial attacks is to find an adversarial example x^{adv} within $B_\epsilon(x) = \{x + \delta : \|\delta\|_p \leq \epsilon\}$, the ϵ -radius ball around an original image x . Another common setting is to find a valid adversarial example with the smallest ℓ_p distance from the original image.

White-box attacks In white-box settings, attackers can access full information of the target model. One strong and popular example is the Projected Gradient Descent (PGD) attack [2], which iteratively applies the following update rule:

$$x_{k+1}^{adv} = \text{Proj}_{B_\epsilon(x)} \left(x_k^{adv} + \eta \text{sign} \left(\nabla_{x_k^{adv}} L(f(x_k^{adv}), y) \right) \right) \quad (1)$$

where $\text{Proj}_{B_\epsilon(x)}(x^{adv}) \triangleq \arg \min_{x' \in B_\epsilon(x)} \|x^{adv} - x'\|_p$, η is the step size, and $L(f(x), y)$ is a loss function, e.g. the margin loss defined as $\max_{i \neq y} f_i(x) - f_y(x)$. To increase the odds of success, the procedure is restarted multiple times with uniformly sampled initial inputs from $B_\epsilon(x)$.

Black-box attacks In black-box settings, the attacker can only obtain outputs of the target model. Black-box attacks can be largely classified into three categories: transfer-based, score-based, and decision-based. Transfer-based attacks craft adversarial examples using surrogate models which approximate the target model, and transfer them to the target model. The surrogate models are typically obtained by training with similar dataset to that used for training the target model. In score-based settings, attackers can know the output scores (logits) of the classifier. On the other hand, in decision-based settings, attackers only can access the output labels of the classifier. For the latter two approaches, attacks are evaluated in terms of query efficiency, i.e. the number of queries to generate an adversarial example and its perturbation size.

Recently, several studies [22–25] exploited surrogate models to estimate the gradients of the loss function of the target model. Some attack methods used random sampling in the input space, such as the decision-based Boundary Attack [17] and the score-based Simple Black-box Attack [18].

3 Output Diversified Sampling

As intuitively presented in Figure 1, random sampling in the input space does not necessarily produce samples with high diversity measured in the output space. To address this problem, we propose Output Diversified Sampling (ODS). Given an image x , a classifier f and the direction of diversification $w_d \in \mathbb{R}^C$, we define the normalized perturbation vector of ODS as follows:

$$v_{ODS}(x, f, w_d) = \nabla_x w_d^\top f(x) / \|\nabla_x w_d^\top f(x)\|, \quad (2)$$

where w_d is sampled from the uniform distribution over $[-1, 1]^C$. Below we show how to enhance white- and black-box attacks with ODS.

3.1 Initialization with ODS for white-box attacks

In white-box settings, we utilize ODS for initialization (ODI) to generate output-diversified starting points. Given an original input x_{org} and the direction for ODI w_d , we try to find the furthest image x from x_{org} by maximizing $w_d^\top (f(x) - f(x_{org}))$ via the following iterative update:

$$x_{k+1} = \text{Proj}_{B(x_{org})}(x_k + \eta_{ODI} \text{sign}(v_{ODS}(x_k, f, w_d))) \quad (3)$$

where $B(x_{org})$ is the set of allowed perturbations, which is typically an ϵ -ball in ℓ_p norm, and η_{ODI} is a step size. When applying ODI to ℓ_2 attacks, we omit the sign function. After some steps of ODI, we start an attack from the image obtained by ODI. We sample a new direction w_d for each restart in order to obtain diversified starting points for the attacks. We provide the pseudo-code for ODI in Algorithm 2 of the Appendix.

One sampling step of ODI costs roughly the same time as one iteration of most gradient-based attacks (e.g., PGD). Empirically, we observe that the number of ODI steps $N_{ODI} = 2$ is already sufficient to obtain diversified starting points (details of the sensitivity analysis are in the Appendix), and fix $N_{ODI} = 2$ in all our experiments unless otherwise specified. We emphasize that ODS is not limited to PGD, and can be applied to a wide family of optimization-based adversarial attacks.

Experimental verification of increased diversity: We quantitatively evaluate the diversity of starting points in terms of pairwise distances of output values $f(x)$, confirming the intuition presented in the left figures of Figure 1. We take a robust model on CIFAR-10 as an example of target models, and generate starting points by ODI and uniform initialization to calculate the mean pairwise distance. Then, the obtained pairwise distance (i.e. diversity) from ODI is 6.41, which is about 15 times larger than that from uniform initialization (0.38). Details are provided in Section C.1 of the Appendix.

3.2 Sampling update directions with ODS for black-box attacks

In black-box settings, we exploit ODS to sample update directions instead of random sampling. Given a target classifier f , we cannot calculate ODS perturbation $v_{ODS}(x, f, w_d)$ because we are not able

Algorithm 1 Simple Black-box Attack [18] with sampling update direction by ODS

```
1: Input: A targeted image  $x$ , loss function  $L$ , a target classifier  $f$ , a set of surrogate models  $\mathcal{G}$ 
2: Output: attack result  $x_{adv}$ 
3: Set the starting point  $x_{adv} = x$ 
4: while  $x_{adv}$  is not adversary do
5:   Choose a surrogate model  $g$  from  $\mathcal{G}$ , and sample  $w_d \sim U(-1, 1)^C$ 
6:   Set  $q = v_{ODS}(x_{adv}, g, w_d)$ 
7:   for  $\alpha \in \{\epsilon, -\epsilon\}$  do
8:     if  $L(x_{adv} + \alpha \cdot q) > L(x_{adv})$  then
9:       Set  $x_{adv} = x_{adv} + \alpha \cdot q$  and break
```

to calculate gradients on the target model f . To approximate the diversity of the target model, we introduce a surrogate model g and calculate ODS vector $v_{ODS}(x, g, w_d)$.

In this paper, we combine ODS with two black-box attacks: decision-based Boundary Attack [17] and score-based Simple Black-box Attack (SimBA [18]). As an example, we provide the pseudo-code of SimBA with ODS in Algorithm 1. In the original paper [18], the authors picked an update direction q randomly from orthonormal candidates Q . We replace it to ODS, as shown in the line 5 and 6 of Algorithm 1. For other attacks, we replace sampling of the attacks in the same way.

In Algorithm 1, we prepare a set of multiple surrogate models and choose a surrogate model per sampling because we empirically found multiple surrogate models make attacks stronger. We choose each model with equal probability in this paper.

Experimental Verification of Increased Diversity: We quantitatively evaluate that ODS yields large changes in the output space of the target model, as shown in the right figures of Figure 1. As the target and surrogate models, we use pre-trained Resnet50 [26] and VGG19 [27] model on ImageNet, respectively. We calculate and compare the mean pairwise distances among samples by ODS and random Gaussian sampling. Then, the obtained pairwise distance (i.e. diversity) by ODS is 0.79, which is 10 times larger than Gaussian sampling (0.07). Details are in Section D.1 of the Appendix.

We also note that ODS does not produce diversified samples when we use random networks as surrogate models, i.e. learned features of images on surrogate models are crucial to transfer diversity.

4 Experiments in white-box settings

In this section, we show that the diversity offered by ODI can improve white-box ℓ_∞ and ℓ_2 attacks. Moreover, we demonstrate that a simple combination of PGD and ODI achieves new state-of-the-art attack success rates. All experiments are held in untargeted settings.

4.1 Efficacy of ODI for white-box attacks

We combine ODI with two popular attacks: ℓ_∞ PGD attack [2] and ℓ_2 C&W attack [28]. We compare the performance of the attacks with ODI against those with naïve initialization.

Setup We perform attacks against three pre-trained models on MNIST, CIFAR-10 and ImageNet, which are adversarially trained with ℓ_∞ PGD attack. For MNIST and CIFAR-10, we use models from MadryLab¹ [2]. For ImageNet, we use the Feature Denoising ResNet152 network² [29].

For PGD attacks, we evaluate the model accuracy with 20 restarts. C&W attacks are evaluated by calculating the minimum ℓ_2 perturbation that yields a valid adversarial example among 10 restarts for each image, and measuring the average of the minimum perturbations.

We sample starting points within $\ell_\infty \epsilon$ -ball and use a uniform distribution for naïve initialization for PGD attacks. For C&W attacks, the original paper [28] did not apply initialization. Here, we sample

¹https://github.com/MadryLab/mnist_challenge and https://github.com/MadryLab/cifar10_challenge. We use their secret model.

²<https://github.com/facebookresearch/ImageNet-Adversarial-Training>.

starting points within ℓ_2 ϵ -ball, and adopt a Gaussian distribution for naïve initialization because it is natural for ℓ_2 sampling. We describe details of settings for each attack in the Appendix.

Table 1: Model performance under attacks with ODI. The values are model accuracy (lower is better) for PGD and the average of the minimum ℓ_2 perturbations (lower is better) for C&W. All results are the average of three trials.

model	PGD		C&W	
	naïve	ODI	naïve	ODI
MNIST	$90.31 \pm 0.02\%$	$90.12 \pm 0.04\%$	2.27 ± 0.00	2.25 ± 0.01
CIFAR-10	$46.06 \pm 0.02\%$	$44.35 \pm 0.03\%$	0.71 ± 0.00	0.67 ± 0.00
ImageNet	$43.5 \pm 0.0\%$	$42.3 \pm 0.0\%$	1.58 ± 0.00	1.32 ± 0.01

Results We summarize all quantitative results in Table 1. Attack performances with ODI are better than naïve initialization for all models and attacks. The improvement by ODI on the CIFAR-10 and ImageNet models is more significant than that of the MNIST model. We hypothesize that this difference results from the difference in model non-linearity. When the non-linearity of a target model is strong, the difference in diversity between the input and output space could be large, in which case ODI will be more effective in providing a diverse set of restarts to facilitate attack algorithms.

4.2 Comparison between PGD attack with ODI and state-of-the-art attacks

To further demonstrate the power of ODI, we perform PGD attack with ODI (called ODI-PGD) against MadryLab’s robust models [2] on MNIST and CIFAR-10, introduced in the previous section, and compare ODI-OGD with state-of-the-art attacks.

Setup One state-of-the-art attack we compare with is the well-tuned PGD attack [16], which achieved 88.21% accuracy for the robust MNIST model. The other attack we focus on is the MultiTargeted attack [16], which obtained 44.03% accuracy against the robust CIFAR-10 model.

We use all test images on each dataset and perform ODI-PGD under two different settings. One is the same as Section 4.1. The other is ODI-PGD with tuned hyperparameters, e.g. increasing the number of steps and restarts. Please see the Appendix for more details of tuning.

Results We summarize the comparison between ODI-PGD and state-of-the-art attacks in Table 2. Our tuned ODI-PGD reduces the accuracy to 88.12% for the MNIST model, and to 44.00% for the CIFAR-10 model. These results outperform existing state-of-the-art attacks.

To compare their runtime, we use the total number of steps (the number of steps multiplied by the number of restarts) as measure of complexity, because the computation time per step is comparable for all gradient-based attacks. In Table 2, the computational cost of tuned ODI-PGD is smaller than that of state-of-the-art attacks, and especially 50 times smaller on the CIFAR-10 model. Surprisingly, ODI-PGD with normal complexity on the first column can even outperform the tuned PGD [16] with high complexity on CIFAR-10. These results indicate the efficiency of ODI.

Table 2: Comparison of ODI-PGD with state-of-the-art attacks against pre-trained defense models. The complexity rows display products of the number of steps and restarts. Results for ODI-PGD are the average of three trials. For ODI-PGD, the number of steps is the sum of ODS and PGD steps.

model		ODI-PGD (in Sec. 4.1)	tuned ODI-PGD	tuned PGD [16]	MultiTargeted [16]
MNIST	accuracy	$90.12 \pm 0.04\%$	$88.12 \pm 0.02\%$	88.21%	88.36%
	complexity	42×20	1050×1000	1000×1800	1000×1800
CIFAR-10	accuracy	$44.35 \pm 0.03\%$	$44.00 \pm 0.01\%$	44.51%	44.03%
	complexity	22×20	160×20	1000×180	1000×180

5 Experiments in black-box settings

In this section, we demonstrate that black-box attacks with sampling by ODS significantly reduce the number of queries needed to generate adversarial examples.

5.1 Query-efficiency of score-based attacks with ODS

To show the efficiency of ODS, we combine ODS with the score-based Simple Black-box Attack (SimBA) [18]. SimBA randomly samples a vector and either adds or subtracts the vector to the target image. The vector is sampled from pre-defined orthonormal vectors in the input space, which are the discrete cosine transform (DCT) basis vectors in the original paper [18]. We replace the DCT basis with sampling by ODS (called SimBA-ODS), as shown in Algorithm 1.

Setup We randomly sample 300 images from ImageNet validation set which are correctly classified. We use pre-trained ResNet50 model as the target model. As surrogate models for ODS, we select four pre-trained models (VGG19, ResNet34, DenseNet121 [30], MobileNetV2 [31]).

We run untargeted and targeted attacks. For targeted attacks, we uniformly sample target labels. We set the same hyperparameters for SimBA as the original paper: step size is 0.2 and the number of iteration is 10000 for untargeted attacks and 30000 for targeted attacks. As the loss function for SimBA, we use the margin loss for untargeted attacks and the cross-entropy loss for targeted attacks.

Results First, we make a comparison between SimBA-DCT [18] and SimBA-ODS. Table 3 compares the number of queries and the median ℓ_2 perturbations. SimBA-ODS remarkably reduces the average queries by a factor ranging between 2 and 3 compared to SimBA-DCT in both untargeted and targeted settings. This confirms that ODS diversity not only is helpful in white-box attacks, but also leads to significant query-efficiencies in black-box settings. Surprisingly, SimBA-ODS also decreases the average perturbations roughly by a factor of two. Namely, the diversity afforded by ODS is also helpful to find natural adversarial examples.

Next, we compare SimBA-ODS with the Square Attack [19], which is state-of-the-art ℓ_∞ and ℓ_2 bounded attacks. For comparison, we regard SimBA as ℓ_2 bounded attacks: the attack is successful when adversarial ℓ_2 perturbation is less than a given bound ϵ . We set $\epsilon = 5$ and other hyperparameters according to the original paper [19], except the number of iteration which is 20000 for untargeted and 60000 for targeted attacks.

Table 3: Number of queries and ℓ_2 perturbations for score-based attacks.

attack	untargeted			targeted		
	success rate	average queries	median ℓ_2 perturbation	success rate	average queries	median ℓ_2 perturbation
SimBA-DCT [18]	100.0%	908	2.95	97.0%	7113	7.00
SimBA-ODS	100.0%	241	1.40	98.3%	3502	3.55

Table 4: Number of queries for SimBA-ODS and ℓ_2 score-based state-of-the-art attacks with norm bound $\epsilon = 5$.

attack	untargeted		targeted	
	success rate	average queries	success rate	average queries
SimBA-ODS	99.67%	236	90.3%	2842
Square [19]	99.67%	647	96.7%	11647

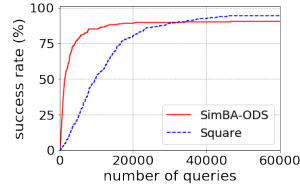


Figure 2: Relationship between success rate and number of queries for targeted score-based attacks.

In Table 4, SimBA-ODS outperforms the Square Attack in terms of the number of queries in both untargeted and targeted settings. For targeted attacks, the attack success rate of SimBA-ODS is lower than the Square Attack because SimBA does not restrict ℓ_2 -norm of adversarial perturbation. To

compare the query-efficiency in target settings more precisely, we depict how the attack success rate increases with the number of queries in Figure 2. The success rate of SimBA-ODS rapidly increases at small query levels compared to the Square Attack.

5.2 Query-efficiency of decision-based attacks with ODS

We demonstrate that ODS also improves query-efficiency for decision-based attacks. We combine ODS with the decision-based Boundary Attack [17]. The Boundary Attack starts from an image which is adversarial, and iteratively updates the image to find smaller perturbations. To generate the update direction, the authors [17] sampled a random noise vector from a Gaussian distribution $\mathcal{N}(0, 1)$ per step. We replace the sampling from a Gaussian distribution with sampling by ODS (called Boundary-ODS). We give the pseudo-code of Boundary-ODS in Algorithm 3 of the Appendix.

Setup We use the same settings as the previous section for score-based attacks: 300 validation images on ImageNet, pre-trained ResNet50 target model, and four pre-trained surrogate models. We run untargeted and targeted attacks. In targeted settings, we give randomly sampled images with target labels as initial images. We use the implementation in Foolbox [32] for Boundary Attack with default parameters, which is more efficient than the original implementation.

We also compare Boundary-ODS with two state-of-the-art decision-based attacks: the HopSkipJump attack [20] and the Sign-OPT attack [21]. We use the implementation in ART [33] for HopSkipJump and the author’s implementation for Sign-OPT. We set default hyperparameters for both attacks.

Results Table 5 summarizes median ℓ_2 perturbations at fixed queries for each attack. Apparently, Boundary-ODS significantly improves query-efficiency compared to the original Boundary Attack. Moreover, Boundary-ODS even outperforms state-of-the-art attacks. The median ℓ_2 perturbation at 10000 queries decreases to less than one-third for untargeted attacks and less than one-fourth for targeted attacks. We also describe the relationship between median ℓ_2 perturbations and the number of queries in Figure 3. Boundary-ODS outperforms other attacks, especially in targeted settings. Boundary-ODS only needs less than 3500 queries to achieve the adversarial perturbation obtained by other attacks at 10000 queries.

Table 5: Median ℓ_2 perturbations for Boundary-ODS and decision-based state-of-the-art attacks.

attack	number of queries					
	untargeted			targeted		
	1000	5000	10000	1000	5000	10000
Boundary [17]	45.07	11.46	4.30	73.94	41.88	27.05
Boundary-ODS	7.57	0.98	0.57	27.24	6.84	3.76
HopSkipJump [20]	14.86	3.50	1.79	65.88	33.98	18.25
Sign-OPT [21]	21.73	3.98	2.01	68.75	36.93	22.43

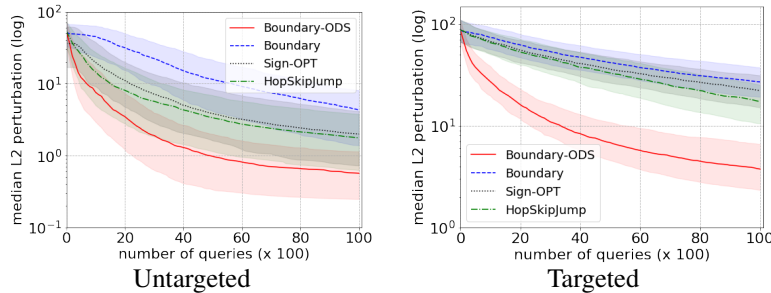


Figure 3: Relationship between median ℓ_2 perturbations and the number of queries for decision-based attacks. Error bars show 25%ile and 75%ile of ℓ_2 perturbations.

5.3 Effectiveness of ODS with out-of-distribution images

Although several studies used prior knowledge from surrogate models to improve performance of black-box attacks, there is a drawback—those approaches require dataset to train surrogate models. In reality, it is impossible to obtain dataset used for training of the target model. However, ODS is applicable even if we only have limited out-of-distribution (OOD) training dataset which only contains images whose labels are different from labels of attacked images and target labels. Under the condition, most existing methods using prior knowledge would not work, because it is difficult to approximate gradients of the loss function on the target model. In contrast, ODS does not need to estimate gradients of the loss function, so it could work with OOD training dataset.

We demonstrate an experiment to confirm the statement. We select 100 classes on ImageNet which are different from classes of images used in the experiments of Section 5.2. We train surrogate models using OOD training dataset with the 100 classes. We train five surrogate models with the same ResNet18 architecture because multiple surrogate models provide diversified directions. Then, we run Boundary-ODS with the trained surrogate models under the same setting as Section 5.2. In Table 6, while Boundary-ODS with OOD training dataset underperforms Boundary-ODS with full dataset, it still significantly outperforms the original Boundary Attack with random sampling. Namely, the diversity by ODS is helpful to improve black-box attacks even if we only have OOD images.

Table 6: Median ℓ_2 perturbations for Boundary-ODS with surrogate models trained with OOD images.

attack	number of queries					
	untargeted			targeted		
	1000	5000	10000	1000	5000	10000
Boundary [17]	45.07	11.46	4.30	73.94	41.88	27.05
Boundary-ODS (OOD dataset)	11.27	1.63	0.98	41.67	13.72	8.39
Boundary-ODS (full dataset in Sec. 5.2)	7.57	0.98	0.57	27.24	6.84	3.76

6 Related works

ODS utilizes the output diversity on target models. A related work in the context is the white-box MultiTargeted attack [16]. The attack changes the target class of attacks per restarts, and it can be regarded as a method which aims to obtain diversified attack results. However, there are several differences between MultiTargeted and ODS. First, while MultiTargeted only focuses on ℓ_p -bounded white-box attacks, ODS is developed for general white- and black-box attacks. In addition, since ODS does not require the original class of target images, ODS gives broader application than MultiTargeted. Furthermore, because the diversity provided by MultiTargeted is restricted to away from the original class, ODS can achieve better results for initialization and sampling than MultiTargeted. We give further discussion in Section E of the Appendix.

ODS utilizes surrogate models, which are commonly used for black-box attacks. Most previous methods exploit surrogate models to estimate gradients of the target model [34–38, 22–25]. In contrast, ODS does not approximate gradients of the loss function, but instead focuses on the diversity of outputs for the target model. As a result, ODS is applicable for out-of-distribution images, as discussed in Section 5.3.

7 Conclusion

In this paper, we propose ODS, a novel sampling strategy for white- and black-box attacks. By generating more diverse perturbations as measured in the output space, ODS brings more effective starting points for white-box attacks. Leveraging surrogate models, ODS also improves the exploration of the output space for black-box attacks. Moreover, ODS for black-box attacks is applicable even if surrogate models are trained with out-of-distribution dataset from target images, so black-box attacks with ODS are more practical than other black-box attacks using prior knowledge of surrogate models. Empirical results demonstrate that ODS with existing attack methods outperforms state-of-the-art attacks in various white-box and black-box settings.

While we only focus on ODS with surrogate models trained with labeled dataset, we believe that ODS works well even if we only have unlabeled dataset. We also suppose that we can improve the efficiency of ODS by the selection of suitable surrogate models via reinforcement learning. We leave them as future works.

Broader Impact

The existence of adversarial examples is a major source of concerns for machine learning applications in the real world. For example, imperceptible perturbations crafted by malicious attackers could deceive safety critical systems such as autonomous driving and facial recognition systems. Since adversarial examples exist not only for images, but also for other domains such as text and audio, the potential impact is large. Our research provides new state-of-the-art black-box adversarial attacks in terms of query-efficiency and makes adversarial attacks more practical and strong. While all experiments in this paper are for images, the proposed method could be applicable to other modalities. Thus, our research could be used in harmful ways by malicious users.

On the positive side, strong attacks are necessary to develop robust machine learning models. For the last few years, several researchers have proposed adversarial attacks which break previous defense models. In response to these strong attacks, new and better defense mechanisms have been developed. It is this feedback loop between attacks and defenses that advances the field. Our research not only provides a state-of-the-art attack, but also sheds light on a new perspective, the importance of the diversity, for strong adversarial attacks, so our research could inspire new approaches to robustness.

Acknowledgements

This research was supported in part by AFOSR (FA9550-19-1-0024), NSF (#1651565, #1522054, #1733686), ONR, and FLI.

References

- [1] Christian Szegedy, Wojciech Zaremba, Ilya Sutskever, Joan Bruna, Dumitru Erhan, Ian Goodfellow, and Rob Fergus. Intriguing properties of neural networks. *arXiv preprint arXiv:1312.6199*, 2013.
- [2] Aleksander Madry, Aleksandar Makelov, Ludwig Schmidt, Dimitris Tsipras, and Adrian Vladu. Towards deep learning models resistant to adversarial attacks. In *International Conference on Learning Representations*, 2018.
- [3] Ian J. Goodfellow, Jonathon Shlens, and Christian Szegedy. Explaining and harnessing adversarial examples. In *International Conference on Learning Representations*, 2015.
- [4] Yang Song, Taesup Kim, Sebastian Nowozin, Stefano Ermon, and Nate Kushman. Pixeldefend: Leveraging generative models to understand and defend against adversarial examples. In *International Conference on Learning Representations*, 2018.
- [5] Pouya Samangouei, Maya Kabkab, and Rama Chellappa. Defense-gan: Protecting classifiers against adversarial attacks using generative models. In *International Conference on Learning Representations*, 2018.
- [6] Andrew Slavin Ross and Finale Doshi-Velez. Improving the adversarial robustness and interpretability of deep neural networks by regularizing their input gradients. In *AAAI Conference on Artificial Intelligence*, 2018.
- [7] Haichao Zhang and Jianyu Wang. Iadversarially robust training through structured gradient regularization. In *Advances in Neural Information Processing Systems*, 2018.
- [8] Seyed-Mohsen Moosavi-Dezfooli, Alhussein Fawzi, Jonathan Uesato, and Pascal Frossard. Robustness via curvature regularization, and vice versa. In *International Conference on Learning Representations*, 2019.

- [9] Chongli Qin, James Martens, Sven Gowal, Dilip Krishnan, Krishnamurthy Dvijotham, Alhussein Fawzi, Soham De, Robert Stanforth, and Pushmeet Kohli. Adversarial robustness through local linearization. In *Advances in Neural Information Processing Systems*, 2019.
- [10] Eric Wong and J Zico Kolter. Provable defenses against adversarial examples via the convex outer adversarial polytope. In *International Conference on Machine Learning*, 2017.
- [11] Aditi Raghunathan, Jacob Steinhardt, and Percy S Liang. Certified defenses against adversarial examples. In *International Conference on Learning Representations*, 2018.
- [12] Jeremy Cohen, Elan Rosenfeld, and Zico Kolter. Certified adversarial robustness via randomized smoothing. In *International Conference on Machine Learning*, 2019.
- [13] Alexey Kurakin, Ian J. Goodfellow, and Samy Bengio. Adversarial machine learning at scale. In *International Conference on Learning Representations*, 2017.
- [14] Tianhang Zheng, Changyou Chen, and Kui Ren. Distributionally adversarial attack. In *AAAI Conference on Artificial Intelligence*, 2019.
- [15] Francesco Croce and Matthias Hein. Minimally distorted adversarial examples with a fast adaptive boundary attack. *arXiv preprint arXiv:1907.02044*, 2019.
- [16] Sven Gowal, Jonathan Uesato, Chongli Qin, Po-Sen Huang, Timothy Mann, and Pushmeet Kohli. An alternative surrogate loss for pgd-based adversarial testing. *arXiv preprint arXiv:1910.09338*, 2019.
- [17] Wieland Brendel, Jonas Rauber, and Matthias Bethge. Decision-based adversarial attacks: Reliable attacks against black-box machine learning models. In *International Conference on Learning Representations*, 2018.
- [18] Chuan Guo, Jacob R. Gardner, Yurong You, Andrew G. Wilson, and Kilian Q. Weinberger. Simple black-box adversarial attacks. In *International Conference on Machine Learning*, 2019.
- [19] Maksym Andriushchenko, Francesco Croce, Nicolas Flammarion, and Matthias Hein. Square attack: a query-efficient black-box adversarial attack via random search. *arXiv preprint arXiv:1912.00049*, 2019.
- [20] Jianbo Chen, Michael I Jordan, and Martin J Wainwright. HopSkipJumpAttack: a query-efficient decision-based adversarial attack. In *IEEE Symposium on Security and Privacy (SP)*, 2020.
- [21] Minhao Cheng, Simranjit Singh, Patrick H. Chen, Pin-Yu Chen, Sijia Liu, and Cho-Jui Hsieh. Sign-opt: A query-efficient hard-label adversarial attack. In *International Conference on Learning Representations*, 2020.
- [22] Jiawei Du, Hu Zhang, Joey Tianyi Zhou, Yi Yang, and Jiashi Feng. Query-efficient meta attack to deep neural networks. In *International Conference on Learning Representations*, 2020.
- [23] Zhichao Huang and Tong Zhang. Black-box adversarial attack with transferable model-based embedding. In *International Conference on Learning Representations*, 2020.
- [24] Yiwen Guo, Ziang Yan, and Changshui Zhang. Subspace attack: Exploiting promising subspaces for query-efficient black-box attacks. In *Advances in Neural Information Processing Systems*, 2019.
- [25] Shuyu Cheng, Yinpeng Dong, Tianyu Pang, Hang Su, and Jun Zhu. Improving black-box adversarial attacks with a transfer-based prior. In *Advances in Neural Information Processing Systems*, 2019.
- [26] Kaiming He, Xiangyu Zhang, Shaoqing Ren, and Jian Sun. Deep residual learning for image recognition. In *IEEE Conference on Computer Vision and Pattern Recognition*, 2016.
- [27] Karen Simonyan and Andrew Zisserman. Very deep convolutional networks for large-scale image recognition. In *International Conference on Learning Representations*, 2015.

- [28] Nicholas Carlini and David Wagner. Towards evaluating the robustness of neural networks. In *Proceedings of the IEEE Symposium on Security and Privacy*, 2017.
- [29] Cihang Xie, Yuxin Wu, Laurens van der Maaten, Alan Yuille, and Kaiming He. Feature denoising for improving adversarial robustness. In *IEEE Conference on Computer Vision and Pattern Recognition*, 2019.
- [30] Gao Huang, Zhuang Liu, Laurens van der Maaten, and Kilian Q. Weinberger. Densely connected convolutional networks. In *IEEE Conference on Computer Vision and Pattern Recognition*, 2017.
- [31] Mark Sandler, Andrew Howard, Menglong Zhu, Andrey Zhmoginov, and Liang-Chieh Chen. Mobilenetv2: Inverted residuals and linear bottlenecks. In *International Conference on Learning Representations*, 2018.
- [32] Jonas Rauber, Wieland Brendel, and Matthias Bethge. Foolbox: A python toolbox to benchmark the robustness of machine learning models. In *Reliable Machine Learning in the Wild Workshop, 34th International Conference on Machine Learning*, 2017.
- [33] Maria-Irina Nicolae, Mathieu Sinn, Minh Ngoc Tran, Beat Buesser, Ambrish Rawat, Martin Wistuba, Valentina Zantedeschi, Nathalie Baracaldo, Bryant Chen, Heiko Ludwig, Ian Molloy, and Ben Edwards. Adversarial robustness toolbox v1.2.0. *arXiv preprint arXiv:1807.01069*, 2018.
- [34] Nicolas Papernot, Patrick McDaniel, and Ian Goodfellow. Transferability in machine learning: from phenomena to black-box attacks using adversarial samples. In *Asia Conference on Computer and Communications Security*, 2017.
- [35] Yanpei Liu, Xinyun Chen, Chang Liu, and Dawn Song. Delving into transferable adversarial examples and black-box attacks. In *International Conference on Learning Representations*, 2017.
- [36] Thomas Brunner, Frederik Diehl, Michael Truong Le, and Alois Knoll. Guessing smart: Biased sampling for efficient black-box adversarial attacks. In *IEEE Conference on Computer Vision and Pattern Recognition*, 2019.
- [37] Jinghui Cai, Boyang Wang, Xiangfeng Wang, and Bo Jin. Accelerate black-box attack with white-box prior knowledge. In *International Conference on Intelligent Science and Big Data Engineering*, 2020.
- [38] Fnu Suya, Jianfeng Chi, David Evans, and Yuan Tian. Hybrid batch attacks: Finding black-box adversarial examples with limited queries. In *29th USENIX Security Symposium (USENIX Security 20)*, 2020.
- [39] Jonathan Uesato, Brendan O’Donoghue, Aaron van den Oord, and Pushmeet Kohli. Adversarial risk and the dangers of evaluating against weak attacks. In *International Conference on Machine Learning*, 2018.
- [40] Diederik P. Kingma and Jimmy Ba. A method for stochastic optimization. In *International Conference on Learning Representations*, 2015.
- [41] Laurens van der Maaten and Geoffrey Hinton. Visualizing data using t-sne. *Journal of machine learning research*, 9, Nov 2008.
- [42] Jonathan Uesato, Jean-Baptiste Alayrac, Po-Sen Huang, Robert Stanforth, Alhussein Fawzi, and Pushmeet Kohli. Are labels required for improving adversarial robustness? In *Advances in Neural Information Processing Systems*, 2019.
- [43] Yair Carmon, Aditi Raghunathan, Ludwig Schmidt, Percy Liang, and John C. Duchi. Unlabeled data improves adversarial robustness. In *Advances in Neural Information Processing Systems*, 2019.
- [44] Haichao Zhang and Jianyu Wang. Defense against adversarial attacks using feature scattering-based adversarial training. In *Advances in Neural Information Processing Systems*, 2019.

- [45] Chengzhi Mao, Ziyuan Zhong, Junfeng Yang, Carl Vondrick, and Baishakhi Ray. Metric learning for adversarial robustness. In *Advances in Neural Information Processing Systems*, 2019.
- [46] Ali Shafahi, Mahyar Najibi, Amin Ghiasi, Zheng Xu, John Dickerson, Christoph Studer, Larry S. Davis, Gavin Taylor, and Tom Goldstein. Adversarial training for free! In *Advances in Neural Information Processing Systems*, 2019.
- [47] Dinghui Zhang, Tianyuan Zhang, Yiping Lu, Zhanxing Zhu, and Bin Dong. You only propagate once: Accelerating adversarial training via maximal principle. In *Advances in Neural Information Processing Systems*, 2019.

A Pseudo-code of proposed methods

In this section, we provide the pseudo-codes of methods proposed in the main paper. First, Algorithm 2 shows the pseudo-code of ODI for white-box attacks in Section 3.1. The line 5-6 in the algorithm describes the iterative update by ODI.

Algorithm 2 Initialization by ODS (ODI) for white-box attacks

- 1: **Input:** A targeted image x_{org} , a target classifier f , perturbation set $B(x_{org})$, number of ODI steps N_{ODI} , step size η_{ODI} , number of restarts N_R
 - 2: **Output:** Starting points $\{x_i^{start}\}$ for adversarial attacks
 - 3: **for** $i = 1$ **to** N_R **do**
 - 4: Sample x_0 from $B(x_{org})$, and sample $w_d \sim U(-1, 1)^C$
 - 5: **for** $k = 0$ **to** $N_{ODI} - 1$ **do**
 - 6: $x_{k+1} \leftarrow \text{Proj}_{B(x_{org})}(x_k + \eta_{ODI} \text{sign}(v_{ODS}(x_k, f, w_d)))$
 - 7: $x_i^{start} \leftarrow x_{N_{ODI}}$
-

We also describe the algorithm of Boundary-ODS, used in Section 5.2 of the main paper. Algorithm 3 shows pseudo-code of Boundary-ODS. The original Boundary Attack [17] first sampled a random noise vector q from a Gaussian distribution $\mathcal{N}(0, 1)$ and then orthogonalized the vector to keep the distance from the original image (line 7 in Algorithm 3). After that, the attack refined the vector q to reduce the distance from the original image such that the following equation holds:

$$d(x, x_{adv}) - d(x, x_{adv} + q) = \epsilon \cdot d(x, x_{adv}) \quad (4)$$

where $d(a, b)$ is the distance between a and b . We replace the random Gaussian sampling to ODS as in the line 5 and 6 of Algorithm 3. Sampled vectors by ODS yield large changes for outputs on the target model and increase the probability that the updated image is adversarial (i.e. the image satisfies the line 9 of Algorithm 3), so ODS makes the attack efficient.

Algorithm 3 Boundary Attack [17] with sampling update direction by ODS

- 1: **Input:** A targeted image x , a label y , a target classifier f , a set of surrogate models \mathcal{G}
 - 2: **Output:** attack result x_{adv}
 - 3: Set the starting point x_{adv} which is adversary
 - 4: **while** $k < \text{number of steps}$ **do**
 - 5: Choose a surrogate model g from \mathcal{G} , sample $w_d \sim U(-1, 1)^C$
 - 6: Set $q = v_{ODS}(x_{adv}, g, w_d)$
 - 7: project q onto a sphere around the original image x
 - 8: update q with a small movement toward the original image x such that Equation (4) holds
 - 9: **if** $x_{adv} + q$ is adversarial **then**
 - 10: Set $x_{adv} = x_{adv} + q$
-

B Details of experiment settings

B.1 Hyperparameters and settings for attacks in Section 4.1

We describe hyperparameters and settings for PGD and C&W attacks in Section 4.1.

Multiple loss functions $L(\cdot)$ can be used for PGD attacks, including the cross-entropy loss, and the margin loss defined as $\max_{i \neq y} f_i(x) - f_y(x)$. We use the margin loss for PGD attacks to make considered attacking methods stronger.

PGD attacks have three hyperparameters: perturbation size ϵ , step size η and number of steps N . We chose $\epsilon = 0.3, 8/255, 4/255$, $\eta = 0.02, 2/255, 0.5/255$ and $N = 40, 20, 50$ for MadryLab (MNIST), MadryLab (CIFAR-10), ResNet152 Denoise (ImageNet), respectively. We use the whole test set except for ImageNet, where the first 1000 test images are used.

For C&W attacks, we define naïve random initialization to make sure the starting points are within an ℓ_2 ϵ -radius ball: we first sample Gaussian noise $w \sim N(0, 1)$ and then add the clipped noise $\epsilon \cdot w / \|w\|_2$ to an original image. We set the perturbation radius of initialization ϵ by reference to attack bounds in other studies: $\epsilon = 2.0, 1.0, 5.0$ for MadryLab (MNIST), MadryLab (CIFAR-10), ResNet152 Denoise (ImageNet), respectively. we also set hyperparameters of C&W attacks as follows: max iterations are 1000 (MNIST) and 100 (CIFAR-10 and ImageNet), search step is 10, learning rate is 0.1, and initial constant is 0.01. The attack is performed for the first 1000 images (MNIST and CIFAR-10) and the first 500 images (ImageNet).

B.2 Hyperparameter tuning for tuned ODI-PGD in Section 4.2

We describe hyperparameter tuning for our tuned ODI-PGD in Section 4.2. We summarize the setting in Table 7.

Table 7: Hyperparameter setting for tuned ODI-PGD in Section 4.2.

model	ODI		optimizer	PGD	
	total step N_{ODI}	step size η_{ODI}		total step N	step size (learning rate) η_k
MNIST	50	0.05	Adam	1000	0.1 ($k < 500$) 0.01 ($500 \leq k < 750$) 0.001 ($750 \leq k$)
CIFAR-10	10	8/255	sign function	150	8/255 ($k < 50$) 0.8/255 ($50 \leq k < 100$) 0.08/255 ($100 \leq k$)

For ODI, we increase the number of ODI step N_{ODI} to obtain more diversified inputs than ODI with $N_{ODI} = 2$. In addition, we make step size η_{ODI} smaller than ϵ on MNIST, because ϵ -ball with $\epsilon = 0.3$ is large and $\eta_{ODI} = 0.3$ is not suitable for seeking the diversity within the large ϵ -ball. In summary, we set $(N_{ODI}, \eta_{ODI}) = (50, 0.05), (10, 8/255)$ for the MNIST model and the CIFAR-10 model, respectively.

We tune hyperparameters of PGD based on Goyal et al. [16]. While several studies used the sign function to update images for the PGD attack, some studies [39, 16] reported that updates by Adam optimizer [40] brought better results than the sign function. Following the previous studies [39, 16], we consider the sign function as an optimizer and the choice of an optimizer as a hyperparameter. We use Adam for the PGD attack on the MNIST model and the sign function on the CIFAR-10 model.

We adopt scheduled step size instead of fixed one. Because we empirically found that starting from large step size brings better results, we set the initial step size η_0 as $\eta_0 = \epsilon$ for the CIFAR-10 model. When we use Adam, step size is considered as learning rate.

B.3 Setting for training on ImageNet in Section 5.3

We describe the setting of training of surrogate models on ImageNet in the experiment of Section 5.3. We use the implementation of training provided in PyTorch with default hyperparameters. Namely, training epochs are 90 and learning rates are changed depending on epoch: 0.1 until 30 epochs, 0.01 until 60 epochs, 0.001 until 90 epochs. Batch size is 256 and weight decay 0.0001.

C Additional results and experiments for ODI with white-box attacks

C.1 Diversity offered by ODI

We empirically demonstrate that ODI can find a more diverse set of starting points than random uniform initialization, as pictorially shown in the left figures of Figure 1 of the main paper.

As an example of target models, we train a robust classification model using adversarial training [2] on CIFAR-10. We adopted popular hyperparameters for adversarial training under the ℓ_∞ PGD attack on CIFAR-10: perturbation size $\epsilon = 8/255$, step size $\eta = 2/255$, and number of steps $N = 10$. Training epochs are 100 and learning rates are changed depending on epoch: 0.1 until 75 epochs, 0.01 until 90 epochs, and 0.001 until 100 epochs. Batch size is 128 and weight decay 0.0002.

On the target model, we quantitatively evaluate the diversity of starting points by each initialization in terms of pairwise distances of output values $f(x)$. Each initialization is bounded within ℓ_∞ ϵ -ball with $\epsilon = 8/255$. We pick 100 images on CIFAR-10 and run each initialization 10 times to calculate the mean pairwise distances among outputs for different starting points. As a result, the mean pairwise distance obtained from ODI is 6.41, which is about 15 times larger than that from uniform initialization (0.38). This corroborates our intuition that starting points obtained by ODI are more diverse than uniform initialization.

We also visualize the diversity offered by ODI. First, we focus on loss histogram of starting points by ODI and naïve uniform initialization. We pick an image from the CIFAR-10 test dataset and run each initialization 100 times. Then, we calculate loss values for starting points to visualize their diversity in the output space. The left panel of Figure 4 is the histogram of loss values for each initialization. We can easily observe that images from naïve initialization concentrate in terms of loss values (around -1.0), whereas images from ODI are much more diverse in terms of the loss values.

In addition, we apply t-SNE [41] to the output logits for starting points by each initialization. We visualize the embedding produced by t-SNE in the right panel of Figure 4. As expected, starting points produced by ODI are more diversified than those by naïve initialization.

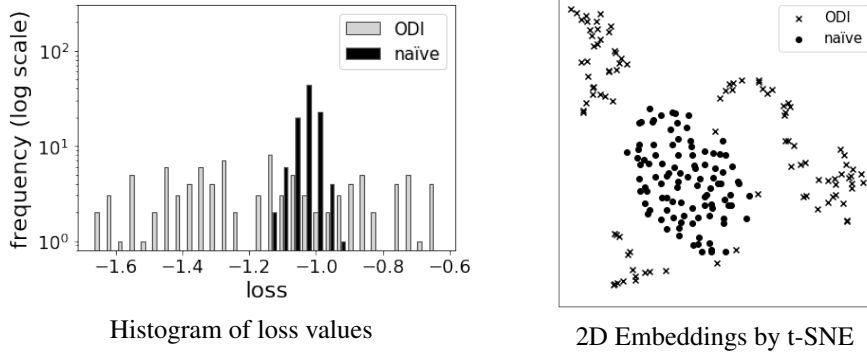


Figure 4: (Left): Histogram of loss values evaluated at starting points by ODI and naïve uniform initialization. The loss function is the margin loss. (Right): Embedding for starting points sampled on each initialization produced by t-SNE.

C.2 Analysis of the sensitivity to hyperparameters of ODI

For ODI, we mainly set the number of ODI steps $N_{ODI} = 2$ and step size $\eta_{ODI} = \epsilon$. To validate the setting, we confirm that ODI-PGD is not sensitive to these hyperparameters. We attack adversarially trained models on CIFAR-10 introduced in Section C.1, and adopt the same attack setup for ODI-PGD on CIFAR-10 as Section 4.1. We test $N_{ODI} = 2, 4, 8, 16$ and $\eta_{ODI} = \epsilon, \epsilon/2, \epsilon/4, \epsilon/8$, but exclude patterns with $N_{ODI} \cdot \eta_{ODI} < 2\epsilon$ to make $N_{ODI} \cdot \eta_{ODI}$ larger than or equal to the diameter of the ϵ -ball. We calculate the mean accuracy for five repetitions of the attack, each with 20 restarts.

Table 8 shows the mean accuracy under ODI-PGD for different hyperparameters. The maximum difference in the mean accuracy among different hyperparameters of ODI is only 0.05%. Although large N_{ODI} and η_{ODI} will be useful to find more diversified starting points, the performance of

Table 8: The sensitivity to the number of ODI steps N_{ODI} and step size η_{ODI} . We repeat each experiment 5 times to calculate statistics.

N_{ODI}	η_{ODI}	mean	max	min
2	ϵ	44.46%	44.50%	44.45%
4	$\epsilon/2$	44.47%	44.50%	44.42%
4	ϵ	44.42%	44.48%	44.40%
8	$\epsilon/4$	44.47%	44.52%	44.44%
8	$\epsilon/2$	44.42%	44.48%	44.36%
8	ϵ	44.46%	44.49%	44.42%
16	$\epsilon/8$	44.46%	44.50%	44.43%
16	$\epsilon/4$	44.46%	44.50%	44.40%
16	$\epsilon/2$	44.45%	44.48%	44.43%
16	ϵ	44.44%	44.47%	44.41%

ODI is not very sensitive to hyperparameters. Thus, we restrict N_{ODI} to a small value to give fair comparison in terms of computation time as much as possible. Table 8 also shows that the difference between the maximum and minimum accuracy is about 0.1% for all hyperparameter pairs. This result supports the stability of ODI.

C.3 Accuracy curve for adversarial attacks with ODI

In Section 4, we experimentally represented that the diversity offered by ODI improved white-box ℓ_∞ and ℓ_2 attacks. we describe the accuracy curve with the number of restarts for attacks with ODI and naïve initialization.

Figure 5 shows how the attack performance improves as the number of restarts increases in the experiment of Section 4.1. Attacks with ODI outperforms those with naïve initialization with the increase of restarts in all settings. These curves further corroborate that restarts facilitate the running of attack algorithms, and ODI restarts are more effective than naïve ones. We note that the first restart of ODI is sometimes worse than naïve initialization. It is because diversity can cause local optima, i.e. random directions of ODI are not always useful. With the increase of restarts, at least one direction is useful and the accuracy drops.

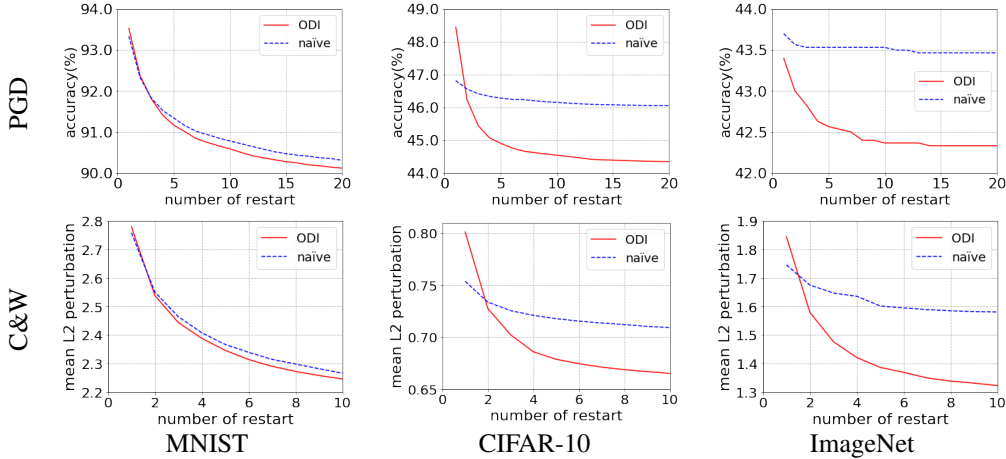


Figure 5: The attack performance against number of restarts for attacks with ODI. (Top): the model accuracy for PGD, (Bottom): the average of minimum ℓ_2 perturbations for C&W.

Next, we describe the accuracy curve for the comparison between state-of-the-art attacks and ODI-PGD in Section 4.2. To emphasize the stability of the improvement, we evaluate the confidence intervals of our results against MadryLab’s MNIST and CIFAR-10 models. We run tuned ODI-PGD attack with 3000 restarts on MNIST and 100 restarts on CIFAR-10. Then, we sample 1000 runs on

MNIST and 20 runs on CIFAR-10 from the results to evaluate the model accuracy, and re-sample 100 times to calculate statistics. Figure 6 shows the accuracy curve under tuned ODI-PGD. We observe that confidence intervals become tighter as the number of restarts grows, and tuned ODI-PGD consistently outperforms the state-of-the-art attack after 1000 restarts on MNIST and 20 restarts on CIFAR-10.

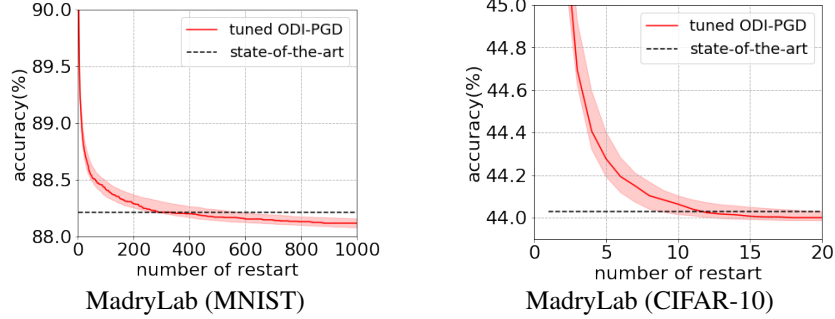


Figure 6: Model accuracy under tuned ODI-PGD and the current state-of-the-art attacks [16]. The solid lines represent values from Table 2 and the error bars show 95% confidence intervals.

C.4 Tighter estimation of robustness for various models

One important application of powerful adversarial attacks is to evaluate and compare different defense methods. In many previous works on defending against adversarial examples, PGD attack with naïve uniform initialization (called naïve-PGD) is a prevailing benchmark and its attack success rate is commonly regarded as a tight estimation on (worst-case) model robustness. In this section, we conduct a case study on six recently published defense methods [42–47] to show that ODI-PGD outperforms naïve-PGD in terms of upper bounding the worst model accuracy under all possible attacks.

Setup We use pre-trained models from four of those studies, and train the other two models [46, 47] using the settings and architectures described in their original papers. We run attacks with $\epsilon = 8/255$ on all test images. Other attack settings are the same as the experiment for CIFAR-10 in Section 4.1. Apart from comparing ODI-PGD and naïve-PGD, we also evaluate PGD attack without restarts (denoted as PGD_1) as it is adopted in several existing studies [42–44, 47].

Table 9: Accuracy of models after performing ODI-PGD and naïve-PGD attacks against recently proposed defense models.

model	(1) PGD_1	(2) naïve-PGD	(3) ODI-PGD	(1)–(2)	(2)–(3)
UAT [42]	62.63%	61.93%	57.43%	0.70%	4.50%
RST [43]	61.17%	60.77%	59.93%	0.40%	0.84%
Feature-scatter [44]	59.69%	56.49%	39.52%	3.20%	16.97%
Metric learning [45]	50.57%	49.91%	47.64%	0.56%	2.27%
Free [46]	47.19%	46.39%	44.20%	0.80%	2.19%
YOPO [47]	47.70%	47.07%	45.09%	0.63%	1.98%

Results As shown in Table 9, ODI-PGD uniformly outperforms naïve-PGD against all six recently-proposed defense methods, lowering the estimated model accuracy by 1–17%. In other words, ODI-PGD provides uniformly tighter upper bounds on the worst case model accuracy than naïve-PGD. Additionally, The accuracy ranking of the defence methods for ODI-PGD is different from naïve-PGD and PGD_1 . These results indicate that ODI-PGD might be a better benchmark for comparing and evaluating different defense methods, rather than naïve-PGD and PGD_1 .

D Additional results and experiments for ODS with black-box attacks

D.1 Diversified samples by ODS

We empirically show that ODS can yield diversified changes in the output space of the target model, as shown in the right figures of Figure 1 of the main paper. Specifically, we evaluate the mean pairwise distance among outputs for different perturbations by ODS and compare it with the distance among outputs for random Gaussian sampling.

We use pre-trained Resnet50 [26] and VGG19 [27] model as the target and surrogate models, respectively. We pick 100 images on ImageNet validation set and sample perturbations 10 times by each sampling method. For comparison, we normalize the perturbation to the same size in the input space. Then, the obtained pairwise distance on the target model by ODS is 0.79, which is 10 times larger than the pairwise distance by random Gaussian sampling (0.07). This indicates that the diversity by ODS is transferable.

D.2 Success rate curve of score-based attacks

In Section 5.1, we demonstrated that SimBA-ODS outperformed state-of-the-art attacks in terms of the query-efficiency. As an additional result, we give the success rate curve of score-based attacks with respect to the number of queries in the experiments. Figure 7 and 8 shows how the success rate changes with the number of queries for SimBA-ODS and state-of-the-art attacks. SimBA-ODS especially brings query-efficiency at small query levels in both untargeted and targeted settings.

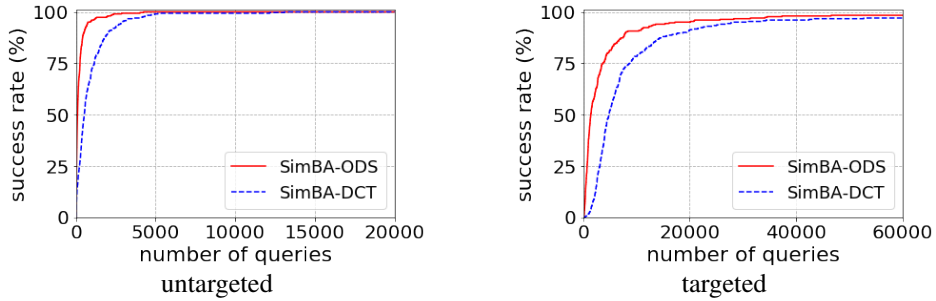


Figure 7: Relationship between success rate and number of queries for score-based SimBA-ODS and SimBA-DCT.

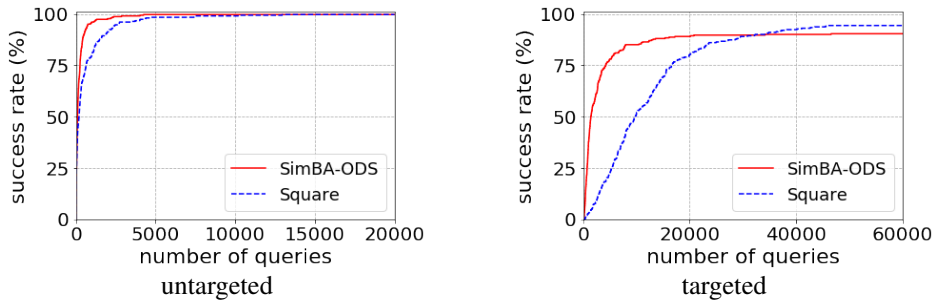


Figure 8: Relationship between success rate and number of queries for score-based SimBA-ODS and Square Attack. Each attack is evaluated with norm bound $\epsilon = 5$.

D.3 Frequency distribution of ℓ_2 perturbation for decision-based attacks

In Section 5.2, we demonstrated that Boundary-ODS outperformed state-of-the-art attacks in terms of median ℓ_2 perturbation. Here, we depict the frequency distribution of the perturbations to show the consistency of the improvement. Figure 9 describes the cumulative frequency distribution of ℓ_2 perturbations for each attack at 10,000 queries. Boundary-ODS consistently decreases ℓ_2 perturbations compared to other attacks in both untargeted and targeted settings.

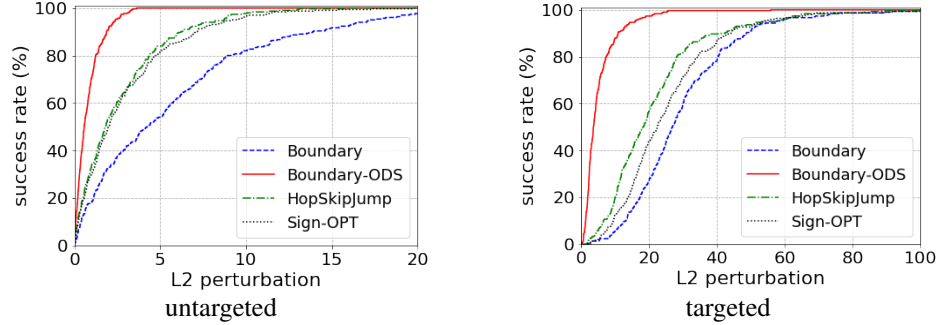


Figure 9: Cumulative frequency distribution of ℓ_2 perturbations at 10000 queries for decision-based attacks.

D.4 Performance of ODS against different target models

In this paper, we used pre-trained ResNet50 model as the target model for all experiments in Section 5. Here we set pre-trained VGG19 model as the target model and run experiments to show that the efficiency of ODS is independent with target models. As surrogate models, we replace VGG19 with ResNet50, i.e. we use four pre-trained models (ResNet50, ResNet34, DenseNet121, MobileNetV2).

We run experiments for SimBA-ODS in Section 5.1 and Boundary-ODS in Section 5.2. All settings except the target model and surrogate models are the same as the previous experiments. In Table 10 and 11, ODS significantly improves attacks against VGG19 model for both SimBA and Boundary Attack. This indicates that the efficiency of ODS does not depend on target models.

Table 10: Query counts and ℓ_2 perturbations for score-based Simple Black-box Attacks (SimBA) against pre-trained VGG19 model on ImageNet.

attack	untargeted			targeted		
	success rate	average query	median ℓ_2 distance	success rate	average query	median ℓ_2 distance
SimBA-DCT [18]	100.0%	618	2.85	100.0%	4090	6.81
SimBA-ODS	100.0%	175	1.35	99.7%	1778	3.31

Table 11: Median ℓ_2 perturbations for decision-based Boundary Attacks against pre-trained VGG19 model on ImageNet.

attack	number of queries					
	untargeted			targeted		
	1000	5000	10000	1000	5000	10000
Boundary[17]	45.62	11.79	4.19	75.10	41.63	27.34
Boundary-ODS	6.03	0.69	0.43	24.11	5.44	2.97

D.5 Effect of the choice of surrogate models

In Section 5.1 and 5.2, we used four pre-trained models as surrogate models. To investigate the effect of the choice of surrogate models, we run attacks with seven different sets of surrogate models. All settings except surrogate models are the same as the previous experiments.

Table 12 and 13 shows results for SimBA-ODS and Boundary-ODS, respectively. First, the first four rows in both tables are results for a single surrogate model. The degree of improvements depends on the model. ResNet34 gives the largest improvement and VGG19 gives the smallest improvement. Next, the fifth and sixth rows show results for sets of two surrogate models. By combining surrogate models, the query efficiency improves, especially for targeted attacks. This means that the diversity from multiple surrogate models is basically useful to make attacks strong. Finally, the performances

in the seventh row are results for four surrogate models, which are not always better than results for the combination of two models (ResNet34 and DenseNet121). When the performances for each surrogate model are widely different, the combination of those surrogate models could be harmful.

Table 12: Query counts and ℓ_2 perturbations for SimBA-ODS attacks with various sets of surrogate models. In the column of surrogate models, R:ResNet34, D:DenseNet121, V:VGG19, M:MobileNetV2.

surrogate models	num.	untargeted			targeted		
		success rate	median query	median ℓ_2 distance	success rate	median query	median ℓ_2 distance
R	1	100.0%	274	1.35	95.3%	5115	3.50
D	1	100.0%	342	1.38	96.7%	5282	3.51
V	1	100.0%	660	1.78	88.0%	9769	4.80
M	1	100.0%	475	1.70	95.3%	6539	4.53
R,D	2	100.0%	223	1.31	98.0%	3381	3.39
V,M	2	100.0%	374	1.60	96.3%	4696	4.27
R,V,D,M	4	100.0%	241	1.40	98.3%	3502	3.55

Table 13: Median ℓ_2 perturbations for Boundary-ODS attacks with various sets of surrogate models. In the column of surrogate models, R:ResNet34, D:DenseNet121, V:VGG19, M:MobileNetV2.

surrogate models	num.	number of queries					
		untargeted			targeted		
		1000	5000	10000	1000	5000	10000
R	1	9.90	1.41	0.79	31.32	11.49	7.89
D	1	10.12	1.39	0.76	32.63	11.30	7.44
V	1	22.68	3.47	1.52	49.18	24.26	17.75
M	1	20.67	2.34	1.10	44.90	18.62	12.01
R,D	2	7.53	1.07	0.61	26.00	8.08	6.22
V,M	2	17.60	1.70	0.92	39.63	14.97	9.21
R,V,D,M	4	7.57	0.98	0.57	27.24	6.84	3.76

D.6 Effect of the number of surrogate models for the experiment in Section 5.3

We described that surrogate models with limited out-of-distribution training dataset are still useful for ODS in Section 5.3. In the experiment, we used five surrogate models with the same ResNet18 architecture. Here, we reveal the importance of the number of surrogate models through experiments with the different number of models. Table 14 shows the result for Boundary-ODS with the different number of surrogate models. With the increase of the number of models, the query efficiency consistently improves.

Table 14: Median ℓ_2 perturbations for Boundary-ODS attacks with different number of surrogate models against out-of-distribution images on ImageNet.

num. of models	number of queries					
	untargeted			targeted		
	1000	5000	10000	1000	5000	10000
1	19.45	2.90	1.66	47.86	25.30	20.46
2	15.45	2.42	1.35	43.45	19.30	13.78
3	13.75	1.96	1.14	41.63	16.91	11.14
4	14.23	1.86	1.21	41.65	14.86	9.64
5	11.27	1.63	0.98	41.67	13.72	8.39

D.7 Score-based attacks with ODS against out-of-distribution images

In Section 5.3, we demonstrated that the decision-based Boundary-ODS attack works well even if we only have surrogate models trained with limited out-of-distribution dataset. Here, we evaluate score-based SimBA-ODS with these surrogate models. Except surrogate models, we adopt the same setting as Section 5.1.

In Table 15, SimBA-ODS with out-of-distribution dataset outperforms SimBA-DCT in untargeted settings. In targeted settings, while SimBA-ODS improves the ℓ_2 perturbation, the average queries for SimBA-ODS are comparable with SimBA-DCT. We hypothesize that it is because ODS only explores the subspace of the input space. The restriction to the subspace may lead to bad local optima. We can mitigate this local optima problem by applying random sampling temporally when SimBA-ODS fails to update a target image in many steps in a low.

We note that decision-based Boundary-ODS with OOD dataset is effective, as shown in Section 5.3. We hypothesize that the difference in effectiveness is because Boundary-ODS does not use scores of the target model and thus does not trap in local optima.

Table 15: Query counts and ℓ_2 perturbations for SimBA-ODS attacks with surrogate models trained with OOD images on ImageNet.

attack	untargeted			targeted		
	success rate	average queries	median ℓ_2 perturbation	success rate	median queries	average ℓ_2 perturbation
SimBA-DCT [18]	100.0%	908	2.95	97.0%	7113	7.00
SimBA-ODS (OOD dataset)	100.0%	490	1.94	94.7%	6924	4.92
SimBA-ODS (full dataset)	100.0%	241	1.40	98.3%	3502	3.55

E Relationship and Comparison between ODS and MultiTargeted

In this section, we describe that ODS gives better diversity than the MultiTargeted attack [16] for initialization and sampling.

MultiTargeted is a variant of white-box PGD attacks, which maximizes $f_t(x) - f_y(x)$ where $f(x)$ is logits, y is the original label and t is a target label. The target label is changed per restarts. In other words, MultiTargeted moves a target image to a particular direction in the output space, which is represented as like $w_d = (1, 0, -1, 0)$ where 1 and -1 correspond to the target and original label, respectively. Namely, the procedure of MultiTargeted is technically similar to ODS.

However, there are some key differences between MultiTargeted and ODS. One of the difference is the motivation. MultiTargeted was proposed as a white-box attack and the study only focused on ℓ_p -bounded white-box attacks. On the other hand, our study gives broader application for white- and black-box attacks. As far as we know, ODS is the first method which exploits the output diversity for initialization and sampling.

Another key difference is the necessity of the original label of target images. ODS does not use the information about the original label, and thus ODS is applicable for black-box attacks even if surrogate models are trained with out-of-distribution training dataset, as shown in Section 5.3. On the other hand, since MultiTargeted exploits the original label of target images to calculate the direction of the attack, we cannot apply MultiTargeted to sampling for black-box attacks against out-of-distribution images.

Finally, the level of diversity is also different. As we mentioned in Section 6, the direction of MultiTargeted is restricted to away from the original class. This restriction could be harmful for diversity because the subspace to explore directions is limited. To show this statement, we apply MultiTargeted to initialization for white-box attacks and sampling for black-box attacks, and demonstrate that ODI provides better diversity than MultiTargeted for initialization and sampling (especially for sampling).

Initialization in white-box settings We apply MultiTargeted to initialization for white-box attacks in Section 4.1. Table 16 represents the comparison of the attack performance with initialization by MultiTargeted and ODI. For PGD attacks, MultiTargeted is slightly better than ODI. We hypothesizes that it is because MultiTargeted was developed as a variant of PGD attacks and the initialization by MultiTargeted also works as an attack method. On the other hand, ODI outperforms MultiTargeted for C&W attacks. In this setting, MultiTargeted does not work as an attack method, and thus the difference in the diversity makes the difference in the performance.

Table 16: Comparison of model performance under attacks with MultiTargeted (MT) and ODI. The values are model accuracy (lower is better) for PGD and the average of the minimum ℓ_2 perturbations (lower is better) for C&W. All results are the average of three trials.

model	PGD		C&W	
	MT	ODI	MT	ODI
MNIST	89.94 \pm 0.07%	90.12 \pm 0.04%	2.26 \pm 0.01	2.25 \pm 0.01
CIFAR-10	44.33 \pm 0.01%	44.35 \pm 0.03%	0.69 \pm 0.01	0.67 \pm 0.00
ImageNet	42.2 \pm 0.0%	42.3 \pm 0.0%	2.30 \pm 0.01	1.32 \pm 0.01

Sampling in black-box settings We use MultiTargeted for sampling on the Boundary Attack in Section 5.2 (called Boundary-MT), and compare it with Boundary-ODS. Table 17 and Figure 10 show the results of the comparison. While Boundary-MT outperforms the original Boundary Attack, Boundary-ODS finds much smaller adversarial perturbation than Boundary-MT.

In Figure 10, Boundary-MT slightly outperforms Boundary-ODS at small queries. We hypothesizes that it is because MultiTargeted not works for providing diversity, but works for the approximation of gradients of the loss function. However, with the number of queries, the curve of Boundary-MT is saturated, and Boundary-MT underperforms Boundary-ODS. This is an evidence that the restriction of directions is harmful for sampling.

Table 17: Median ℓ_2 perturbations for Boundary Attack with ODS and MultiTargeted (MT).

attack	number of queries					
	untargeted			targeted		
	1000	5000	10000	1000	5000	10000
Boundary [17]	45.07	11.46	4.30	73.94	41.88	27.05
Boundary-ODS	7.57	0.98	0.57	27.24	6.84	3.76
Boundary-MT	7.65	2.20	2.01	28.16	18.48	16.59

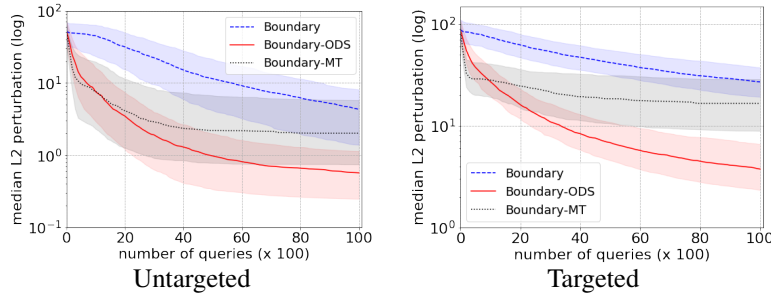


Figure 10: Relationship between median ℓ_2 perturbations and the number of queries for Boundary Attack with ODS and MultiTargeted. Error bars show 25%ile and 75%ile of ℓ_2 perturbations.